High resolution measurement of striation patterns and sarcomere motions in cardiac muscle cells

John W. Krueger and Adam Denton
The Albert Einstein College of Medicine, 1300 Morris Park Avenue, Bronx, New York 10461

ABSTRACT We describe an extension of the method of Myers et al. (1982) to measure with high precision the uniformity of contractile motions that occur between sarcomeres in the isolated cardiac muscle cell (guinea pig and rat). The image of the striations, observed with modulation contrast microscopy, was detected by a linear array of photodiodes. Sarcomere length was measured >500/s from the frequency of the array's video signal at two selectable regions of the cell. A precision test grating demonstrated that method resolves known differences in the spacing between two contiguous striations to ±0.01 μm and that the effects of image translation and microscopic resolution are minor. The distribution of striation spacing appears to be discrete in isolated segments of the cell, and patches of fairly uniform length can be identified that are laterally contiguous. When electrically triggered, contraction is synchronous and the sarcomeres shorten and relengthen smoothly. The contrast between the striations is transiently enhanced during relengthening, an indication that the contracting cell can not be treated as a simple grating. Pauses that occur during late in relengthening (and transient contractile alternans) are characterized by very synchronized activity. These forms of irregular contractile behavior are not explained by desynchronization of a mechanism of release of intracellular calcium. A companion article describes application of the technique to study the nonuniform motions that occur between sarcomeres (Krueger, Denton, and Siciliano, *Biophysical Journal*, 61:145–160, companion manuscript).

INTRODUCTION

Most commonly, uniform shortening is sought when studying the sarcomeric basis of cardiac function. However, the nature of its asynchronous or nonuniform motions provides useful information as well which, for example, can test whether alterations in contraction can be attributed to the desynchronization of intracellular calcium release (3, 4), or whether nonuniformity masks detailed features of the sarcomere's dynamics (29). From another perspective, the organization of the striations in the cell should reflect either patterns of activation or restraints imposed by its cytoskeletal components.

The microscopic details of shortening can be inferred by several methods, yet no one method appears well suited to measure the motions between sarcomeres. Nonuniform contraction of isolated cells is easily detected by light diffraction (16), but the motions can not be localized nor quantified. Cinemicroscopy and computer-based video imaging techniques (26, 30, 31) provide spatial information but do not give satisfactory dynamic resolution with the convenience that experiments in contraction require.

Address correspondence to Dr. John W. Krueger, Department of Physiology & Biophysics, Albert Einstein College of Medicine, Bronx, NY 10461.

Dr. Denton's current address is AT&T Bell Laboratories, Middletown, NJ 07748.

The spatial frequency content of a myocyte's striated image is inversely related to sarcomere length. Accordingly, a special electronic circuit known as a phase-locked loop can be used to convert the frequency of a video signal to a voltage that is inversely proportional to the length of the sarcomere. This method permitted the distribution of sarcomere length to be measured directly from television images of isolated cells (5–7). However, sampling is constrained by the relatively slow field rate (50–60 Hz) of television systems, and resolution is often limited by the image retention and geometric nonlinearity. The self-scanned linear array of photodiodes provides excellent geometric linearity, and the light available in bright field microscopy permits very high speed sampling of sarcomere length (27). But in this case the aperture of the condenser is reduced, image formation is dominated by diffraction processes, the precise association between image intensity and object structure is lost, and the striated patterns may disappear upon contraction (7). The resolution in detecting the motion of individual striations with the phase-locked loop method has not been established. Questions exist about the effect of image translation (1, 11) that have not been tested explicitly.

We applied a phase-locked loop technique (27) to measure sarcomere length nearly simultaneously in two separate, selectable parts of the isolated cardiac cell. Using a precision nonuniform test grating, we show that

the method can measure sarcomere motions with surprising precision. The method also measures the contrast between the striations, because activation influences the cardiac striation's appearance (19). For this reason the striations are visualized with Hoffman modulation contrast microscopy (9), where the intensity in the image can be related to specific structural attributes of the sarcomere. Application of the method reveals that a curious organization of the striations exists, and it tests whether delays in relaxation and contractile alternans arise from desynchronized activation. A companion paper describes an extension of the approach that visualizes asynchronous motion of the striations in order to examine further the mechanical nature of their interconnections (18).

Preliminary descriptions of this method have been presented elsewhere (15, 17).

METHODS

Isolated cardiac muscle cells

Single, Ca^{2+}-tolerant heart cells were isolated from the ventricles of adult rats and 350-g male guinea pigs using the general technique described elsewhere (16, 24). Isolated single cells were stored at room temperature in a Hepes-buffered, physiological salt solution (composition, in mM: NaCl, 118; KCl, 4.8; K_2HPO_4, 1.2; $MgSO_4$, 1.2; Glucose, 11; NaHepes, 25; $CaCl_2$, 1.0 to 2.0, pH 7.4). All observations were made at room temperature (22–23°C).

General experimental apparatus

The cells were placed in a polypropylene microscope chamber (total volume = 1 ml) filled with this Hepes-buffered physiological salt solution. The chamber was placed on the rotating stage of an inverted microscope, and the cells were examined with a 40×, 0.75 numerical aperture (N.A.) water immersion Hoffman modulation contrast objective (Carl Zeiss) and an 0.90 N.A. condenser that was dipped into the experimental solution. The aperture in the modulation contrast system was oriented at 45 degrees with respect to the long axis of the cell in order to provide uniform resolution of the cell's structure. The cells were illuminated by a 50 W halogen lamp that was attenuated by a heat filter. The image of the cell was projected through the third tube of the microscope onto a photodiode array (Reticon 256C/17) that was scanned 526/s. The image was projected from the third tube of the microscope using a 5× ocular and deflected horizontally by a front surface mirror through two converging lenses onto the array. Adjustment of effective focal length (12–13 cm) of the relay lens assembly permitted fine scaling of the image onto the array.

The cells were electrically stimulated to contract with a 3–5 ms, negative-polarity pulse using a micropipet (tip diameter 1–2 μm) that was filled with the bath solution and positioned within 10–20 μm of the cell. A platinum wire dipped into the solution on the opposite side of the chamber served as the reference electrode. Initial sarcomere length was read from a digital voltmeter. The signals representing sarcomere length and the degree of the amplitude modulation of the video signal were stored on FM tape for retrospective analysis. In other cases, the sarcomere length was sampled directly and analyzed by a microcomputer.

Direct measurement of sarcomere length by FM detection

The circuit that we used to measure intracellular sarcomere dynamics is based on the approach for video FM detection using the self-scanned photodiode as described by Myers et al. (27). The array was scanned 526/s, a rate that permitted the striations to be detected by the lower light levels available with the use of a standard 50 W illuminator coupled with modulation contrast microscopy. The original approach (27) was extended to permit measurement of (*a*) motions between sarcomeres and (*b*) the changes in the contrast of the striated pattern.

1. Measurement of sarcomere length in different regions of the cell. Fig. 1 illustrates the relationships between the electronic signals that are used to compute sarcomere length. A block diagram of the circuit is shown in Fig. 2, and a more detailed description of the circuit is given in the Appendix. Sarcomere length is obtained from a measurement of the period of the video waveform as follows. An FM demodulator (i.e., phase-locked loop) is used to measure the frequency of the photodiode's video signal; its output is a 'phase error' signal whose voltage is directly proportional to the instantaneous frequency of the video signal. The phase error signal is integrated over the computational interval (i.e., 'window') and the result is divided into the integral of time for the sampling window. The result of this division is a voltage that is proportional to the average period of the video signal during the computation interval and is thus equivalent to the average sarcomere length in the selected part of the cell. We used two independently adjustable windows that permit two computation intervals per scan (Fig. 1 *B*). The separation between the centers of the windows generally ranged between 15 to 30 μm, and the temporal difference between sampling is only 0.5 to 1 ms. Thus, sarcomere length is recorded nearly simultaneously in two distinct and selectable regions of the cell, as shown in Fig. 1 *C*.

2. Sampling of striations. Two areas of the cell are typically sampled by the array, as represented by the black rectangles in Fig. 1. With the 40× objective lens, the array (6,500 × 432 μm) surveys a path on the specimen that is 58 μm long and <4 μm wide. Typically, each scan includes about 30 striations, or about one-half the length of the average myocyte. From the total magnification (×112) and the numerical aperture of the microscope, the axial resolution can be estimated to be ~6 μm (8). When the first window is set at its largest dimension (or automatically displaced along the array (18)), the device samples an area that is equivalent to ⅛th of the cross section and 1/16th the volume of a typical cardiac cell. The discrete resolution on the photodiode array is equivalent to 0.22 μm/element. The fundamental frequency content of the striations (1/[2.00] to 1/[1.50], i.e. 0.50 to 0.67 lines/μm) is well below the limit imposed by application of the Nyquist criteria (1/[2 × 0.22 μm] = 2.27 lines/μm) in discrete sampling theory. Moreover, the waveform of the striations' intensities presents a continuous function that is spatially filtered by the microscope's optics, the individual elements of the array integrate any local gradient in intensity, the discrete transitions between the pixels are filtered electronically, and the resulting waveform is over sampled by the rapid, repetitive scanning of the array. For these reasons precision must be established experimentally.

3. Striation contrast. The approach also detects of the amplitude modulation of the video signal ('AM', Fig. 1 *B*). A measurement of difference between the intensity of light in the *A* band and the *I* band is obtained by rectification of the video signal (Fig. 2). This voltage is averaged during the computation interval to obtain a signal that is proportional to the average *A–I* difference in the selected part of the cell. The method can detect changes in the contrast between the striations during contraction, as shown in Fig. 1 *E*, and it reveals that

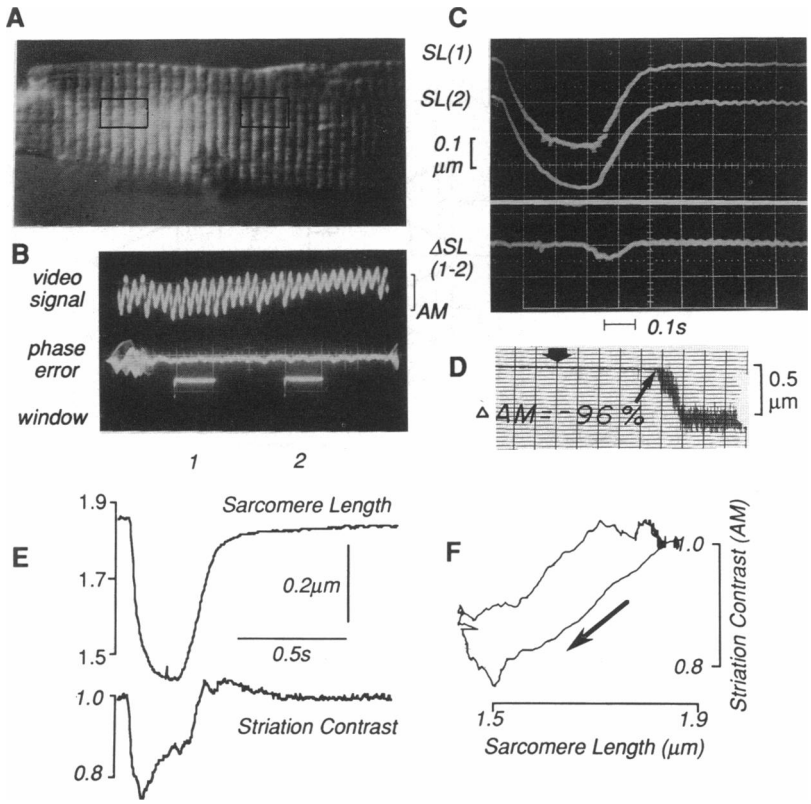

FIGURE 1 Measurement of sarcomere length at two positions by FM detection. (*A*) The appearance of an isolated myocyte visualized by Hoffman modulation contrast microscopy (as photographed from videomonitor; *SL* = 1.92 μm). The rectangles denote two areas selected for sarcomere length measurement. (*B*) Video signal (negative polarity) from the photodiode array from the same striations shown above. The phase error signal is a frequency demodulated voltage that is proportional to the video signal's frequency content at any respective location on the array; the initial instability at the leading edge of the scan represents the time required for lock of the phase-locked loop. 'Window' denotes separately adjustable intervals, 1 and 2, where the phase error signal is integrated to compute sarcomere length. (*C*) The time course of sarcomere shortening in another cell which was electrically stimulated to contract. SL(1) and SL(2) correspond to the sarcomere length measured in the respective windows; 'ΔSL' is the difference in sarcomere length (1–2, 0.1 μm/division). (*D*) Stability of the length measurement when contrast was reduced by lowering the intensity of illumination a 2.0 μm grating, starting from 100% at the broad arrow. Simultaneous recording of contrast (not shown) indicated that striation spacings was constant until contrast was reduced by 96%. (*E*) Time course of sarcomere shortening and the characteristic changes in their contrast during contraction in a guinea pig myocyte. Contrast, denoted by 'AM' in *B*, represents the amplitude of the difference in the intensities which arises from the individual A and I bands as averaged over window 1. (*F*) Dependence of the relative changes in contrast in *E* upon sarcomere length. Contrast is enhanced at short lengths and/or during relengthening, and it is restored slowly in late relaxation. The arrow indicates the direction of contractile changes.

contrast is not uniquely related to sarcomere length (Fig. 1 *F*). Application of the circuit verified that a typical change in the contrast of the striations does not affect the sarcomere length measurement. As demonstrated in Fig. 1 *D*, the measurement of striation spacing remained essentially independent of a decrease in illumination until their contrast was reduced by a least 90%. This limit is >4× the change in the sarcomere's contrast that typically occurs during contraction of the cell (Fig. 1 *F*).

Construction of a nonuniform test grating

The performance of the device was tested with a precision test grating, constructed at the National Nanofabrication Facility (Cornell University) by electron beam lithography and standard fabrication techniques. Briefly, borosilicate microscope slides (Fisher, Gold Seal) were coated with two positive resists and a chromium conductive layer to prevent electron beam divergence. The resists were exposed using an advanced electron beam lithography system (JEOL JBX-5DII[U]) that has a deviation <30 nm, and the pattern was written using a line width of 0.40 μm. After removal of the chromium and development of the exposed resist, the slide was coated with a 1,000 Å layer of aluminum. Finally, the unexposed resist was removed and the slides were cleaned by oxygen ionization.

The essential features of the grating that are relevant to performing the test are shown in Fig. 3 *A*. The grating consists of a uniform reference patch of 50 parallel vertical lines, 700 μm long, that are spaced precisely 2.00 μm apart. Immediately adjacent to these striations were 11 uniform 'test' patches of 50 lines, 40 μm long, whose

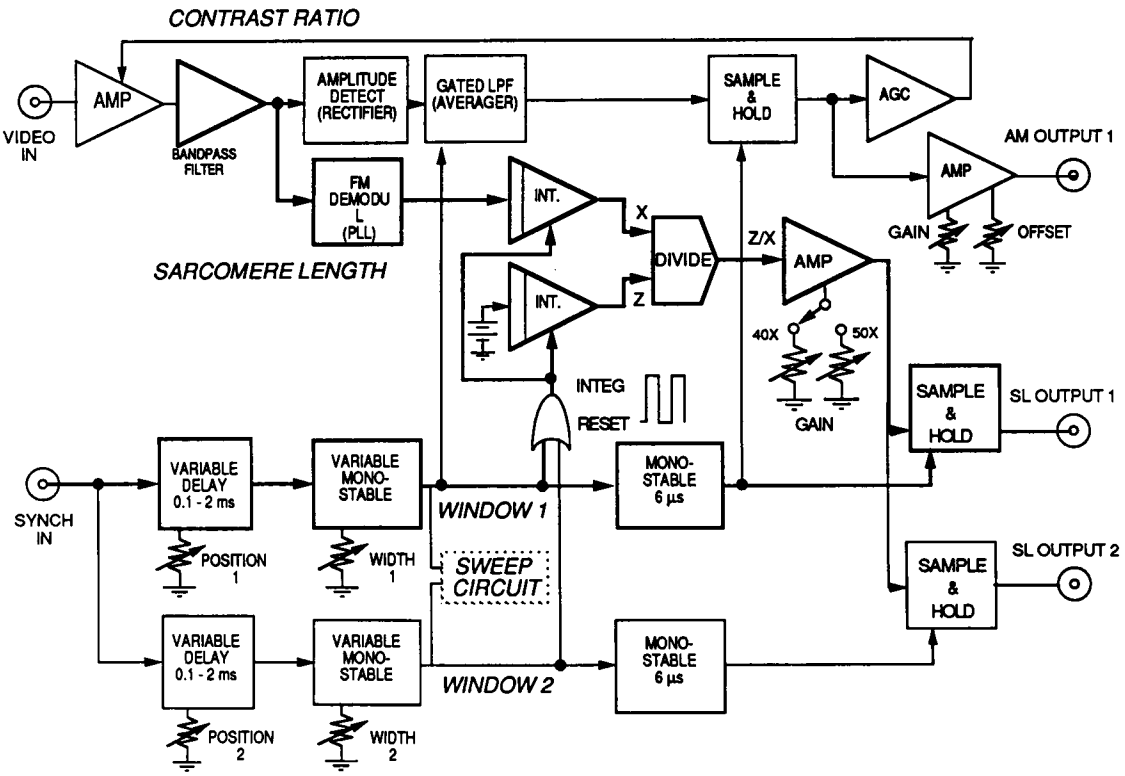

FIGURE 2 Block diagram of the circuit for the detection of the spacings and the appearance of the striated pattern. Components denoted by bold lines correspond to the method described by Myers et al. (1982). Refer to text for details. *PLL*, phase-locked loop; *INT*, integrator; *AGC*, automatic gain control; *AMP*, amplifier; *DIV*, divider; *INT*, integrator. Dashed box denotes circuitry described in the companion study (18).

spacings range between 1.50 and 2.50 μm in 0.10 μm increments to cover the expected range of sarcomere motions. Finally, two other test patches were included with striation spacings of 1.20 and 3.00 μm that are near the extremes of the lock range of the phase-locked loop. The first striation of each test patch was separated from the reference patch by 2.00 μm, while each test patch was vertically separated by a 10 μm clear space (Fig. 3*A*). The clear space enables the precise line associated with the step change in striation spacing to be identified, even though this difference may be less than the resolution of the microscope lens. The relation between spacing of the striations in the test grating, *ss*, and striation spacing measured by the phase locked loop, *PLL*, for all 13 test patches ($1.20 < ss < 3.00$ μm) was: $PLL = 1.02\,ss + 0.04$ ($R^2 = 0.996$), where R is the coefficient of variation in linear regression.

RESULTS

Evaluation of measurement of nonuniform striation spacings

It has been calculated that the phase-locked loop measures mean sarcomere length to a precision $<0.1\%$ (27) when a large window is used to sample the striations. This consideration, however, does not establish the ability of the method to resolve localized changes in sarcomere length in the smaller samples we used or when nonuniformity exists. The resolution of nonuniform motions depends upon (*a*) the response time of the circuit and (*b*) the ability to detect changes in spatial frequencies that are below the classical limit of resolution of the light microscope. As detailed in the Appendix, the expected response time of the circuit spans an interval of 1.14 μm, which is approximately three-fourths of the shortest striation spacing expected in the isolated heart cell.

1. Resolution of localized differences in sarcomere length. The principal uncertainty in detecting nonuniformity is the ability to resolve a difference between contiguous striations that is below the theoretical limit of resolution of the microscope, as emphasized by others (31). By this criteria, the limit of resolution (d) of the 40×, 0.75 N.A. objective is ~ 0.52 μm, given that $d = \lambda/2$ N.A., where λ is the mean wavelength of the illumination (taken as 0.55 μm), and N.A. is the combined numerical aperture of the microscope's objective and condenser lens that is achieved when the modulation contrast aperture oriented 45 degrees with respect to the long axis of the cell. However, this criteria for resolution is not relevant to

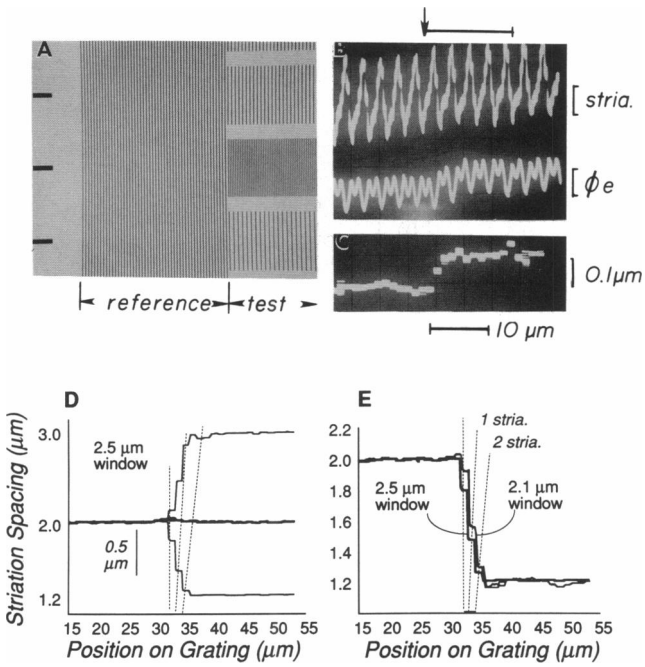

FIGURE 3 Test of the method's resolution of a step response. (*A*) Appearance of a small portion of the optical grating. Patches of striations at right have uniform spacings corresponding to 2.40, 2.50, 1.20, and 3.00 μm. These are separated by 2.00 μm from the 2.00 μm reference patch at left. A 10 μm clear vertical space between each respective test patch helps to identify the precise striation associated with the change in spacing. (*B*) Traces of the video signal (stria., −20 mV/division) and the phase error signal (Φ*E*, 0.1V/division) in response to a step change in striation spacing from 2.00 to 2.10 μm (horizontal calibration: 0.1ms/division; bars = 10 μm). The arrowhead denotes the minimum intensity associated with the first striation at the longer spacing (Hoffman modulation contrast). (*C*) The computed striation spacing that was displayed as the first window was automatically displaced across the test field. Each point represents an overlay of multiple, sequential computations of striation spacing every 1.9 ms at 1.2 μm intervals on the object, where spatial resolution is imposed by the width of the window (2.0 μm). Thus, the response to one striation will require at least two computations. The horizontal scale differs in *B* and *C*. (*D* and *E*) Displays of the step response of striation spacings similar to that in *C*, but measured (*a*) in large transitions between the test patches and (*b*) with only one full scan of the field. Dashed lines denote position of a striation after the transition.

the precision with which object detail can be positioned within the microscopic field (34), and so the precision of measuring sarcomere length must be determined empirically.

Fig. 3 *B* shows the response of the phase error signal to a step change in striation spacing of 0.10 μm in the test grating, i.e., when the transition between 2.0 and 2.1 μm patches was inspected. The phase error signal responds with the first striation at the new spacing and achieves a new steady level within two striations. It is difficult to assess precision by this response alone because the phase error signal contains ripples that arise because of the nature of the method used to detect frequency. An additional feature of the circuit (cf. 18) displays the striation spacing as the sample window is automatically displaced in 1.2 μm increments along the image with each new scan of the array, as shown in Fig. 3 *C*. When the width of the sample window is set to its minimum = 2.0 μm, the measured striation spacing agrees to within ±0.01 μm of the expected value after two-to-three computations, i.e., with a displacement of 2.4-to-3.6 μm in sampling position that would be required to survey two complete striations (Fig. 3 *C*). Thus, the method detects the absolute spacing of each striation to a precision of 0.02 μm, a value that is only 4% the limit of resolution of 0.5 μm that we attribute to our microscope. A comparable precision (*a*) also characterizes a large (0.5 μm) step change to a longer striation spacing (e.g., 2.50 μm, Fig. 3 *D*) but, (*b*) required two striations at the largest transition to shortest spacing tested (i.e., a 0.7- μm step to 1.20 μm, Fig. 3 *D*). A slight increase in window width smooths the result but does not appreciably alter the step response (Fig. 3 *E*). Thus, the method (*a*) performs well over both the smallest and the largest changes in striation spacing that might be anticipated, and (*b*) detects a difference in striation spacing to a precision that is 10 times better than the discrete sampling resolution (0.22 μm) of the individual elements of the array.

One-to-two intermediate points arise in the transition to the new spacing because the striation spacing is computed as a running average of two consecutive striations (the effect being greater at shorter sarcomere lengths). Two histograms of striation spacings that were obtained by full scans with the narrowest window of (*a*) a field including the 2.0 and 1.9 μm patches, and (*b*) a field including the 2.0 and 2.1 μm patches are superimposed in Fig. 4 *A*. The dispersion of each, taken as the width at half amplitude, is ∽0.02 μm. The dispersion of scans restricted to the uniform patches in the test grating (1.2 ≤ striation spacing ≤ 2.1 μm) was 0.028 ± 0.006 μm. This value is within the <30 nm deviatio n expected in the construction of the grating. Consequently, the narrow histograms reiterate that the method appears to detect the spacings in individual striations with an accuracy of ±0.01 μm, or ±0.5% sarcomere length.

The microscopic resolution of the striations had surprisingly little effect on the precision of measuring their spacing. Fig. 4 *B* illustrates the histograms obtained from the 1.9 to 2.0 μm transition as visualized by bright field illumination with the condenser set to its maximum aperture setting of 0.9. In this test, scanning was confined to only two striations in the region of transition, i.e., the last striation before the transition was compared with the second striation occurring at the new

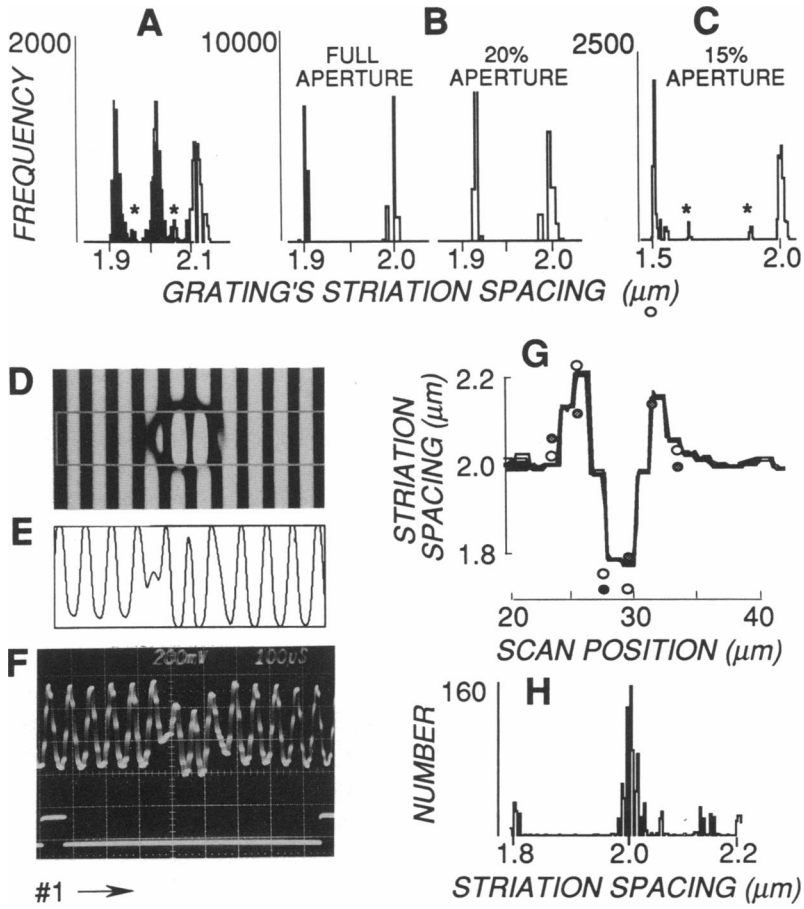

FIGURE 4 Effect of resolving power of the microscope. (*A*) Superimposed histograms obtained from scanning the 1.9 and 2.0 μm patches and the 2.0 and 2.1 μm patches in the grating. The asterisk denotes intermediate points that occur at the transition between striation spacings. (*B*) Minimal effect of reducing the aperture of illumination. The scan was restricted to the last striation before the step and the second striation at the new spacing; the intermediate point was removed from the histogram. (*C*) The spacings measured at a reduced aperture with multiple scans of all consecutive striations in the 2.0 and 1.5 μm patches. (*D*) Appearance of a predictable fluctuation in the 2.0 μm spacings caused by a small oil drop, as visualized by a CCD camera. (*E*) Average intensity pattern in the area outlined in *D* that corresponds to the area sampled by the self-scanned array (resolution = 29.1 pixels/striation). (*F*) Appearance of the video signal from the photodiode array (200 mV/division; resolution = 8.8 diodes/striation). #1 denotes the width and the initial position of the sampling window that was displaced during scanned sampling of striation spacing. (*G*) Relation between computed striation spacing and scanning position. Solid lines were obtained from multiple scans of the phase-locked loop; symbols represent sarcomere length obtained using either centroid (*closed*) or peak (*open*) of the waveform obtained from the CCD in *E*. (*H*) Histogram showing the characteristic trimodal distribution of striation spacings in *G*. Hoffman modulation contrast, *A*; Bright field, *B*, *C*, and D.

spacing, while the intermediate point was removed. Reduction of the condenser aperture by 80% noticeably degraded the sharpness of the striations, as expected by the decreased microscopic resolution. Surprisingly, the lowered resolution did significantly slow the step response in striation spacing (data not shown) nor broaden the dispersion (Fig. 4 *B*). The change in striation spacing (Fig. 4 *B*) is slightly reduced but remains within the precision we attribute to the method. Fig. 4 *C* shows the histogram obtained by full field scans of the 2.0-to-1.5 μm transition when the aperture of the condenser was reduced by 85%. In this case all points were included, and the histogram appeared identical to that obtained at full aperture (not shown).

2. Effect of discrete sampling of a fluctuation in striation spacing. A second question is whether a localized heterogeneity might cause a tracking error with the phase-locked loop? To examine the effect of a predictable fluctuation in striation spacing, a small oil drop was placed over a field of uniform striations (Fig. 4 *D*). The appearance of the fluctuation was sampled simultaneously by the photodiode array and a high resolution CCD camera (CCD72, 768 × 493 elements; Dage MTI). Fig. 4 *E* shows the appearance of the video signal from

the CCD camera, sampled at a resolution of 29.1 pixels/striation, and Fig. 4 *F* shows that from the array where the resolution was only 8.8 diodes/striation. The patterns agree well despite the threefold difference in discrete sampling. The fluctuation in the spacings and the corresponding histogram that were obtained by the phase-locked loop are shown in Figs. 4 *G* and *H*, respectively. The fluctuating sequence of the striation spacings, measured by both methods, are superimposed in Fig. 4 *G*. This comparison emphasizes that the PLL method will underestimate the amplitude of a discrete fluctuation because (*a*) it represents a running average of two contiguous striations, and (*b*) the fundamental frequency it detects reflects the centroid of an oscillation rather than its peak. However, this test also demonstrates that a fluctuation is tracked accurately and gives rise to a characteristic and diagnostic histogram.

3. Translation effects. Because sarcomere length is determined by integration of the rippled phase error signal over a prepositioned sampling interval (Fig. 5, *A* and *B*), displacement of either the sample position or of the striations will generate a small fluctuation when a ripple translates in the optical field. The magnitude of this effect has been debated (1, 11, 28) and so it was tested directly. For these tests the mirror deflecting the image into the relay lenses was replaced by a reflecting prism that was mounted on a servo-controlled galvanometer (model CCX-100; General Scanning, Watertown,

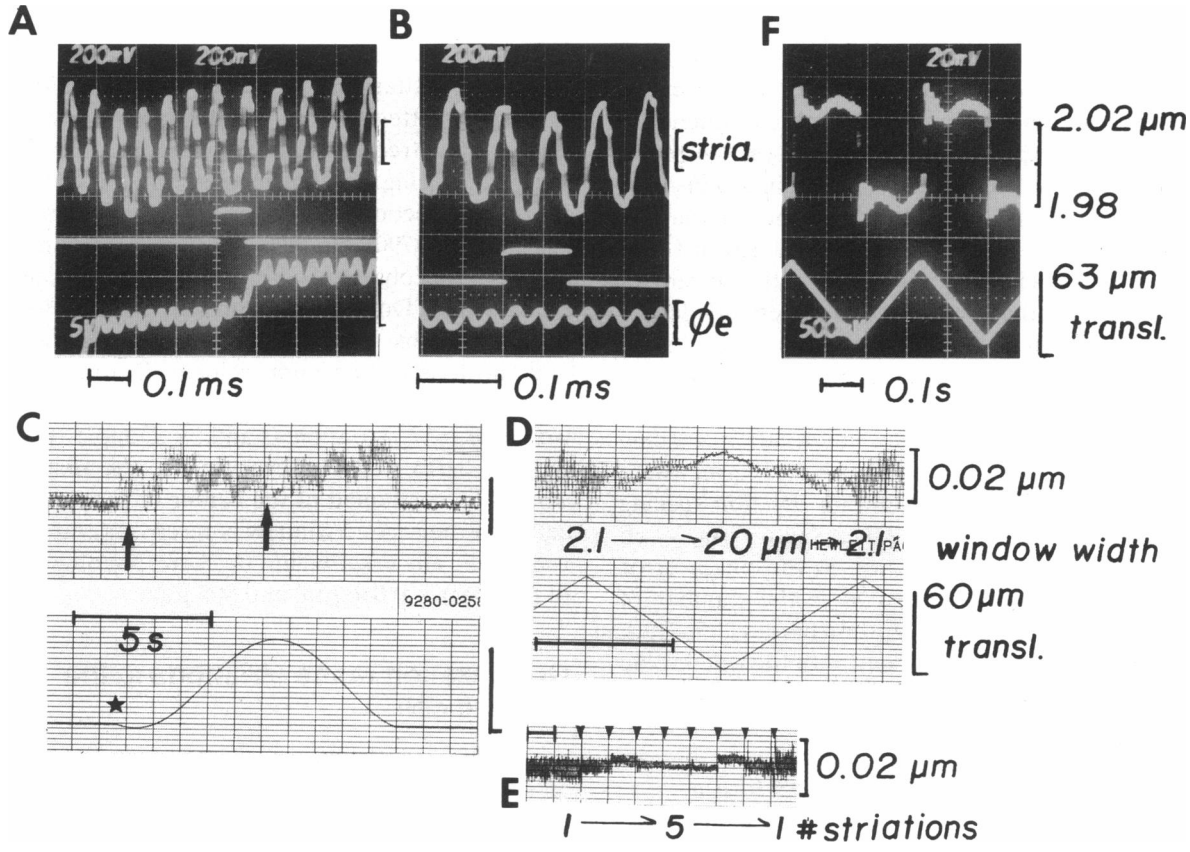

FIGURE 5 Translation effects in measurement of striation spacing. (*A*) Appearance of video signal and phase error signal (Φe – 1.2 V, 200 mV/division) obtained from the 2.0 to 2.5 μm transition in the test grating viewed in bright field. The left edge of the window is aligned with the first striation at 2.5 μm. (*B*) Adjustment of sampling window width (integration interval) to 2.5 μm to encompass 2.5 oscillations of the phase error signal at a striation spacing = 2.0 μm. Video signal has been filtered on the display at 100 kHz (HF 3dB point) in *A* and *B*. (*C*) Chart recordings of striation spacing in response to a sinusoidal displacement of the bright field image of 2.0 μm grating, sampled with the 2.5 μm window shown in *B*. Asterisk denotes onset of displacement. Arrows denote discrete fluctuations corresponding to ripple in phase error signal at the lowest velocity of translation. Secondary oscillations of ~1 s period correspond to variations that are within the dispersion of the grating. (*D*) Effect of manually changing the width of the sampling window during displacement at constant velocity of the image of the 1.8 μm grating (Hoffman modulation contrast). Window width was varied between its minimum width of ~2.1 μm to 20 μm. All calibration scales are the same in *C* and *D*. (*E*) Effect of manually widening the window in increments of one striation, small arrowheads (1 mm/s chart speed, 2 mV/division; Hoffman microscopy). (*F*) Example of a Doppler shift in striation spacing with displacement of the image of the 2.0 μm grating at high velocity (±196 striations/s).

MA). The deflection of the image was controlled with a waveform generator, detected capacitively, and displayed with striation spacing as shown Figs. 5, *C* and *D*.

For evaluation of translation effects, we need consider only the situation when the width of the sampling window is set so that a minimum number of oscillations is included in the integration period (11). Specifically, the amplitude of any fluctuation due to translation should be maximal when the integration period includes an integral number of oscillations, *N*, and one-half of another (11). In our system, the frequency of the phase error signal is twice that of the striations, and with bright field illumination of the grating the signal approximates a sinusoid when the striations are <2.0 μm (Fig. 5, *A* and *B*). Therefore the integration period was set to encompass $N + \frac{1}{4}$ striations, or 2.5 oscillations of the phase error signal. This case occurs when the image of the 2.0 μm grating is translated across a sample window that is 2.5 μm wide (Fig. 5 *B*). Deflection of the image indicated fluctuations occurred at twice the frequency of the striations, as expected for the ripple on the phase error signal (data not shown). Deflection in a sinusoidal pattern reveals the peak amplitude of the fluctuation, which is identified when translation is slowest (cf. *arrows,* Fig. 5 *C*). This was taken to be the maximum fluctuation artifact that we could experimentally define.

In 10 tests, the peak-to-peak amplitude of the maximum fluctuation artifact was equivalent to 0.018 ± 0.0025 μm (±SD). With a purely sinusoidal phase error signal, the expected fluctuation in striation spacing should approximate $k \cdot (\Delta\Phi E/\pi \cdot m) = 0.019$ μm, where k is the slope of the relation between striation spacing and the phase error signal at 2.0 μm (1.63 μm/V, cf. Appendix), $\Delta\Phi E$ is the fluctuation in the phase error signal ($\sim$0.09 V, Fig. 5 *A*), and m is the number of oscillations included in the integration period, 2.5. Thus, the fluctuation is in good agreement with the small value expected. When the window width is increased to 5.0 μm, or twice the worst case tested, the error due to translation should be less than the precision that we attribute to the method; i.e., $0.018/2 < \pm 0.01$ μm.

As expected from the nature of the phase detection, the ripple in the phase error signal becomes more complex when the video signal departs from a sinusoid. This became evident in bright field when the striations are >2.1 μm, as can also be seen in Fig. 5 *A*, or when Hoffman modulation contrast microscopy is used (e.g., Fig. 3 *B*). Therefore we considered a second worst-case situation, i.e., when (*a*) the width of the sampling window was varied continuously during displacement of the image at constant velocity and (*b*) the striations were visualized by modulation contrast. In these observations, the initial width of the window was set to its minimal value $\sim$2.1 μm, and then it was manually varied between 20 and 2.1 μm in proportion to the displacement of the 1.8 μm grating (Fig. 5 *D*). The peak amplitude of the fluctuation was <0.016 μm (Fig. 5 *D*) in this protocol which should span all combinations of phase effects in the integration period. Because the definition of the striations of the cardiac sarcomeres in modulation contrast lies between the extremes shown for the grating, we conclude that translation effects are insignificant. Finally, manually altering the width of the windows shows that increasing the number of striations sampled in the stationary image has minimal effect (Fig. 5 *E*). Thus, any variation in the number of striations sampled during contractile shortening should have little effect.

4. Doppler effects. The detected striation spacing must be larger (or smaller) than the true value when they are translated in the same (or opposite) direction as the scan of the array. When the velocity of translation of the 2.00 μm grating alternates between ±196 striations/s, the spacing is shifted by 0.05 μm (Fig. 5 *F*). Given that the fundamental frequency at 2.00 μm = 15,790 cycles/s, the striation spacing (*ss*) that results from the translation in the same direction as the scan can be calculated as $ss = (2.00\ \mu m)(15790)/(15790 - 196) = 2.025$ μm. Consequently, the observed shift (±0.025 μm) can be explained by a Doppler mechanism. If a cell 100 μm in length contains $\sim$50 striations, is attached at one end, and shortens at maximum velocity (5 μm/s/striation), then the maximum velocity of translation at the free end would be $\sim$125 striations/s and the Doppler shift would be only 0.016 μm. However, in use the first sampling window is positioned of the center of shortening in the cell, and the second window is rarely separated by >30 μm. Thus, any error would be correspondingly reduced to $(30/100) \times 0.016$ μm, or 0.005 μm.

Organization of the striations in the isolated cell

Sarcomere length was measured in both windows in guinea pig cells that were isolated from nine hearts and bathed in solutions containing 1–2 mM calcium. Single cells were selected on the basis of (*a*) a video signal containing well defined striations and (*b*) a stable phase error signal. In 36 cells that were selected without regard to the uniformity of the phase error signal, the average of the sarcomere length in each window was 1.892 ± 0.036 and 1.883 ± 0.042 (μm ± SD). The average of the absolute differences between the windows was 0.021 ± 0.019 (μm ± SD), a value in fair agreement with the dispersion of the method.

Fig. 6 *A* represents the histogram of sarcomere lengths, as sampled in a scanned segment of an intact cell. The

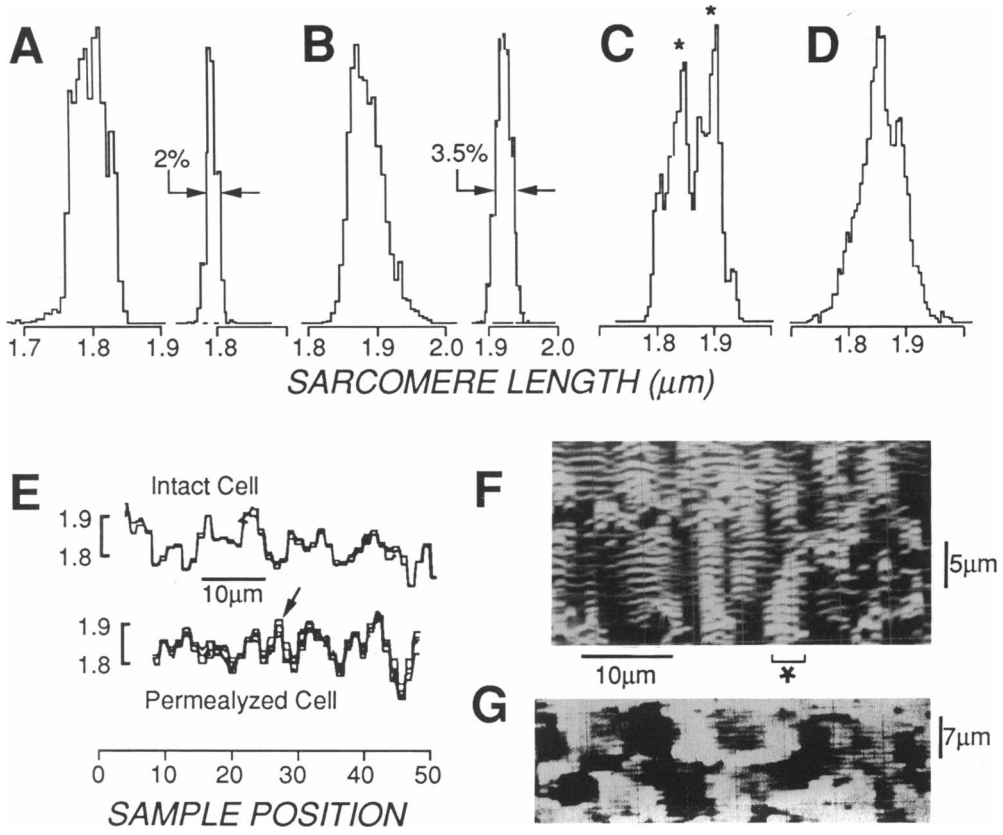

FIGURE 6 Distribution of sarcomere lengths in segments of isolated guinea pig myocytes. (*A*) Example of a narrow distribution of sarcomere length in a scanned intact cell, and the relatively narrow histogram that is obtained when length is sampled over one striation. (*B*) Distribution of sarcomere length in a segment of a permealyzed heart cell and the histogram of fluctuating lengths that was recorded at one point. (*C*) Histogram showing discrete bimodal (*asterisks*) distribution of sarcomere lengths in a scanned segment of an intact cell. (*D*) Distribution of sarcomere lengths at the same region in *C* that was obtained by changing the focus during data acquisition. All histograms represent 10,000 data points. Isolated dropouts that reflect interactions between sampling and the bin width of the computer's histogram display were removed. (*E*) Longitudinal pattern that shows typical, discrete variations of sarcomere length in intact cells. Arrow denotes fluctuations in comparable scans from a detergent-treated cell (multiple scans are shown). (*F* and *G*) Two-dimensional scans showing patch-like organization of sarcomere length in (*F*) an intact and (*G*) a permealyzed cell. *Patch. Refer to text for details.

distribution appears sharp, with little deviation at the shortest or longest sarcomere lengths. The average dispersion in the scanned segments, measured as the full width of the histogram at half its amplitude, was 0.072 ± 0.017 μm (±SD, $N = 34$ histograms; range 0.04 to 0.120 μm). Measurement of sarcomere length at an isolated point on the cell indicates that little methodological deviation occurs which would broaden the histogram.

Sarcomere length in cells exposed to a solution containing nonionic detergent (0.5% wt/vol Brij 58), 5 mM EGTA and 5 mM ATP (19) appeared longer (1.975 ± 0.031 μm, $N = 25$). Although stable in the intact cell (Fig. 6*A*), the phase error signal often fluctuated at specific sites after disruption of the cell membranes. The location of these fluctuations coincided with the occurrence of small particles located in the I band of individual sarcomeres. In this case the shape of the histogram appeared to be more Gaussian with a broader distribution at the extremes, and restriction of sampling to the region of fluctuation resulted in a distribution that also appear to be broadened (Fig. 6*B*). The shape of either histogram is not comparable to that expected to a static fluctuation in striation spacing (cf. Fig. 4*H*). Consequently, after the cell is disrupted by detergents nonsarcomeric remnants are free to fluctuate by Brownian motion, and the distribution of sarcomere lengths may be broadened artefactually.

Discrete sarcomere lengths. The distribution of sarcomere lengths in segments of intact cells appeared discrete and often bimodal. Fig. 6 *C* illustrates a representative histogram from an intact cell that was obtained by continuously scanning a 58 μm long segment. Chang-

ing focus throughout data acquisition to sample the overlying and underlying striations minimized the subpopulations and restored a more normal distribution of striations spacings (Fig. 6 *D*). When sarcomere length in the scanned segment appeared uniform, the distributions were discrete with little spread at the extremes. When the distributions were nonuniform, sarcomere length appeared to cluster in a discrete manner. In some cells, individual discrete subpopulations occurred without overlap in some histograms (not shown). Thus the dispersion within each subpopulation may be appreciable less than that attributed to the cell as a whole.

In these intact, quiescent cells, a small but stable spatial variation of the phase error signal often occurred every three to four striations. The variation in phase error signal migrated with the striations during contractile translation and it was not seen in the uniform gratings. Thus, these variations represent 'quasi periodic' differences in sarcomere length that occur in patches of approximately three to six striations, as illustrated in Fig. 6 *E*. Importantly, the appearance of these scans differs from the triphasic change in length (cf. Fig. 4 *G*) or symmetrical trimodal histograms (cf. Fig. 4 *H*) that characterize a discrete fluctuation. Because a seemingly periodic variation in the length of contiguous striations also appears in records of others (cf. reference 6, Fig. 3 *A*; reference 33, Fig. 4), we asked whether the amplitude of the transition was random? In histograms that showed discrete distributions, the average transition in sarcomere length was 0.052 ± 0.014 μm (±SD, $N = 79$ subpeaks; histograms obtained from 17 cells).

Two-dimensional organization of the striation pattern

A second question is whether the location of the transitions is random or whether the cell's nonmyofibrillar components might artefactually produce the patches of sarcomere organization? If true, particles or a termination of a row of mitochondria should obliterate any organization between laterally adjacent scans of the striations. For this test, sarcomere length was obtained by automatically scanning the narrowed sampling window along the length of the cell (18). At the same time the image of the cell was displaced laterally across the array by the servo-controlled galvanometer to sample the full width of the cell. Analogous to a television display, the intensity of a CRT was modulated by the sarcomere length; the horizontal deflection on the CRT display was determined by the longitudinal position of scanned sampling; and the vertical deflection on the CRT display was determined by the lateral position of the galvanometer-deflected image.

Sampling by this method reveals patches where sarcomere length is similar, as shown in Fig. 6 *F*. The patches remain discrete and have a lateral dimension that exceeds the ~4 μm width of the cell that is scanned by the array, and so the longitudinal variation in striation spacing also has a lateral organization. Increasing the width of the sampling window smooths but otherwise does not alter the basic nature of this pattern. The patches run in rows; i.e., a result not expected if the transition in sarcomere length arose artefactually by a termination of a single row of mitochondria. Rows of patches also skewed and intermingled laterally. Both results are difficult to account for by particulate matter that we would have expected to exert a more idiosyncratic influence on the lateral registration of these patterns. Patches also existed in cells that were exposed to 1% detergent, a step that dramatically lowers the refractive index of the cell due to the dispersion of mitochondrial protein (19). For nine intact and nine detergent-treated cells, the longitudinal spacing between contiguous patches was 8.8 ± 2.28 μm (100 patches) and 9.6 ± 1.26 μm (70 patches) (±SD, mean per cell), respectively.

Synchronous sarcomere shortening in electrically stimulated contracting cells

Sarcomere shortening was studied in segments of unattached cells that were preselected by the sharp appearance of their striations and a stable phase error signal. One window was positioned near the center of the shortening, and the second to sample a patch of uniform length as revealed by the phase error signal. When contraction was triggered by an electrical stimulus the course of sarcomere shortening appeared smooth (Fig. 1, *C* and *E*). Smooth shortening at one site was often associated with similar shortening at the second; thus smooth shortening can not be associated with asynchronous contraction of the cell (Fig. 1 *C* and 7). Conversely, when nonsteady sarcomere shortening was found, it was invariably associated with a combination of two factors: (*a*) a localized variation in the phase error signal near the edge of the window, and (*b*) translation of a region of nonuniformity into or out of the sampling field. Nonsteady shortening was altered by changing the level of focus, and it was not synchronized with the course of shortening in the adjacent window. Thus, nonsteady shortening can not be attributed to synchronized shortening within the isolated heart cell.

Cells in which the variation in the initial sarcomere length occurred between the sample regions also shortened synchronously, while the largest discrepancies in the synchrony of contractile motions existed during the phase of relengthening (cf. Fig. 1 *C*). Examples were

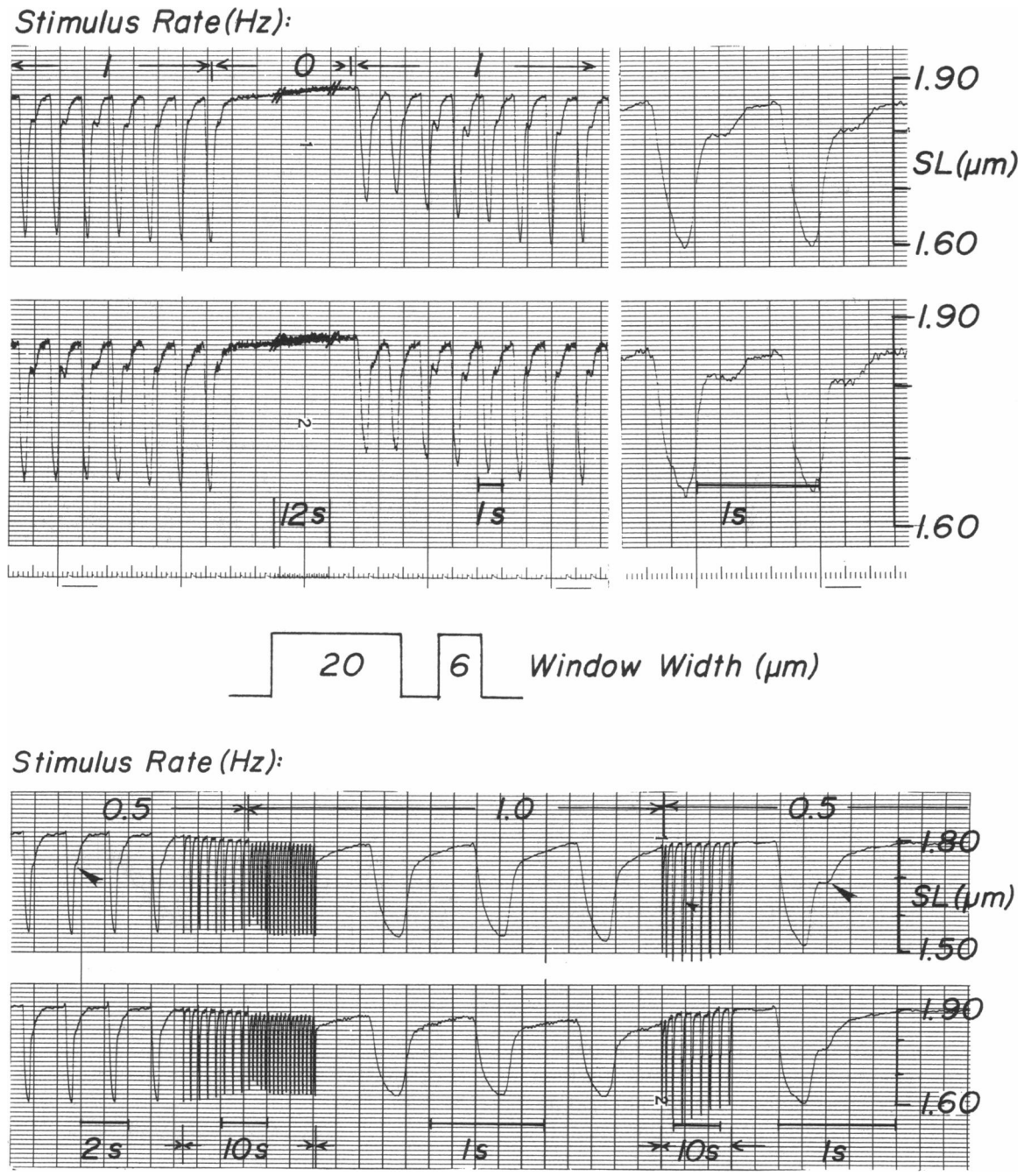

FIGURE 7 Uniform synchronous relengthening during spontaneous 'pauses' in sarcomere relaxation in an electrically stimulated cell. (*Top*) Sarcomere length changes that occur simultaneously in two regions of a single guinea pig myocyte with 'pauses' in late relaxation. The smooth relengthening of the cell in the absence of stimulation shows that these pauses are not due to spontaneous activity. A record at higher chart speed is at right. (*Bottom*) Stimulation at higher rate rapidly abolished the preceding pauses in relaxation denoted by the arrows, an effect that is soon reversed by slowing stimulus rate. Virtually all features of the sarcomere motions are well synchronized in all cases.

found where cells became either more uniform or less so at the peak of shortening, and so we can conclude only that the greatest divergence of sarcomere motions occurred during early relengthening. Cells in which sarcomere length appeared initially uniform tended to shorten reproducibly. In cells where the initial sarcomere length was nonuniform, however, the amplitude of the regions of nonuniform phase error signal tended to be amplified

in repeated contractions, and the sarcomere motions were less reproducible.

Synchronous delays in relaxation and alternating contractions

Relaxation in the isolated unattached cell is characterized by two discrete phases during which relengthening appears to be exponential (13, 16, 21). However, an additional component of relaxation often appears wherein relengthening appears delayed at or near the onset of the second, slower phase. As shown in Fig. 7, these pauses in relengthening appeared to be well synchronized throughout the cell throughout the phase of transition to this behavior, and they were not accompanied by similar pauses during shortening. Similar synchronous events late in relaxation were observed in 24 cells isolated from 14 guinea pig hearts. The initial sarcomere length in this group was 1.886 ± 0.035 μm (mean ± SD), and so there is no indication that this event reflects an increase in the resting level of myoplasmic calcium [ion]. A similar delay in relaxation has been observed previously in isolated guinea pig myocytes by edge detection methods (2) insofar as it is commonly elicited when stimulus rate is lowered and disappears upon stimulation at higher rate (Fig. 7, *bottom*). Because the courses of relengthening are identical in separate regions of the isolated cell, the pauses in relaxation necessarily represent synchronized contractile behavior. Spontaneous shortening was not present when the stimulation was stopped.

Occasionally, isolated cells are also found in which the degree of shortening spontaneously alternates in successive electrically triggered contractions. Fig. 8 illustrates the sarcomere shortening behavior which occurred during a period of transient alternating contractile shortening after the onset of stimulation following a quiescent period of 8 s. Comparison of the amplitude of sarcomere shortening in the separate parts of the cell indicates that contraction was very synchronous during alternating contractions as well as during the phase of adjustment to stable contractile behavior. Alternans behavior was observed in only 5 of more than 100 cells observed.

DISCUSSION

We have demonstrated that sarcomere length can be measured reliably to a precision that is significantly below the limit of resolution of the light microscope (Fig. 3). Using a test employing a relatively large (1.0 μm) increment in striation spacing, Roos and Brady (31) have obtained high resolution measurements based upon the detection of the striation's edge. They attributed precision in the sarcomere length measurement largely to the optimization of (*a*) the contrast sensitivity to the sensor and (*b*) the resolution of the light microscope (31). Our approach is based upon the detection of the position of the A band as detected by its optical gradient (9). We find that precision of the technique is not greatly affected by the definition of the striations that is imposed by the microscope's resolution. Notably,

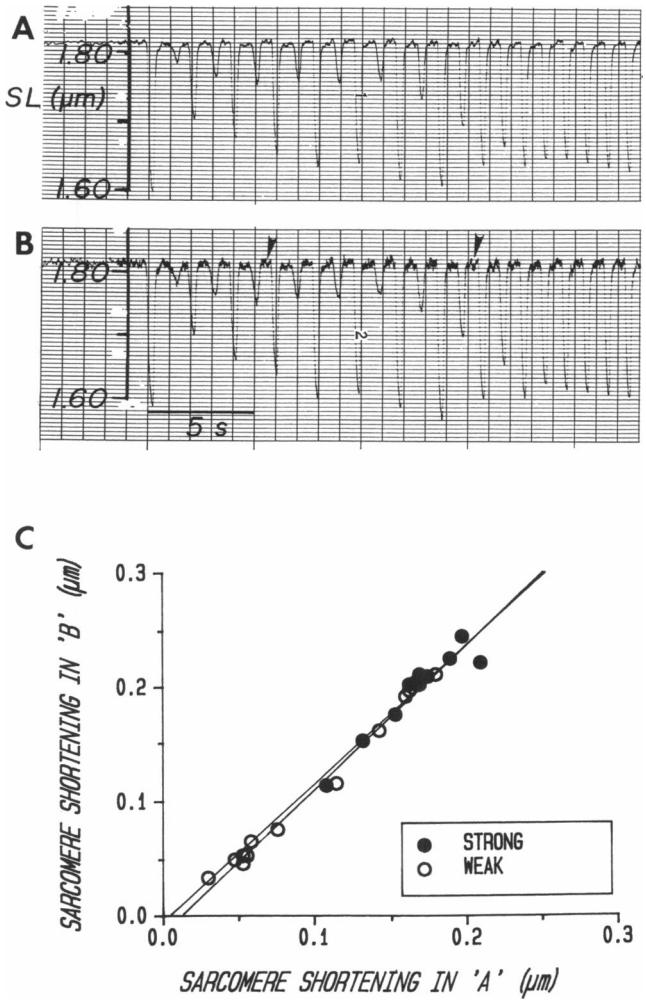

FIGURE 8 Synchronous, uniform shortening in during contractile alternans. (*A* and *B*) Sarcomere shortening in two separate regions of a guinea pig cell during transient period of alternating contractile behavior after the onset of stimulation following a quiescent period of 8 s. (*C*) Comparison of sarcomere shortening in separate parts of the cell during the alternating contractions. Separate lines represent fits by linear regression linear with slopes of 1.22 and 1.24. Both the amplitudes and the synchrony of sarcomere motions agree well between strong and weak contractions and throughout the adjustment to stable behavior. Arrows denote very small scale (~0.01 μm) synchronous motions that may be a recording artifact, because they appear to be well correlated between the separate regions but do not depend on the width of the sampling window.

the step response to exceedingly small differences in striation spacing (i.e., 0.1 μm) was not compromised by severely limiting the condenser aperture, i.e., conditions that noticeably degraded the image and which would have been expected to limit resolution by ~70%. These results are consistent with the fact that (*a*) the criteria for limiting microscopic resolution may not apply to the precision with which object detail can be positioned within the microscopic field (34) and (*b*) the separation of specific features of interest well exceeds the wavelength of light. Consequently, the length of individual sarcomeres can be determined to a precision that likely encroaches upon the very definition of their ultrastructural regularity.

Sarcomere organization in the cardiac cell

The distribution of sarcomere length has been previously found to be relatively broad and fairly Gaussian in the single cardiac cell. The basis for this conclusion is obtained by the averaging of many measurements of sarcomere length that are sampled throughout the cell (6, 32). However, if intracellular elastic elements were to restrain the cardiac sarcomere, we would not expect the distribution to be normal when length is sampled in smaller segments of the cell. When sarcomere length scans were confined to a limited depth and segment of the cardiac cell equivalent to 1/16th its volume, they appear narrower and sharper than prior reports (6, 32), and they often showed evidence for a discrete distribution (Fig. 5).

Discrete spacings also occur in the subcomponents of the light diffraction pattern of the isolated cardiac cell (23). Discrete components in diffractometry require that patches of similar sarcomere length be organized in a spatial and coherent fashion, but the method provides no basis to characterize any pattern uniquely. We find repeating, laterally connected patches in which uniform sarcomere length is uniform. The points of deflection of the phase error signal remained discrete and translated with the sarcomeres' displacements during contraction. Moreover, no comparable pattern was seen in the uniform test gratings (Fig. 4). Thus, it seems unlikely that the spatial periodicity results from aliasing due to discrete sampling by individual elements in the array or tracking errors with the method.

The transition in sarcomere length separating the patches prompted us to measure the spacings of adjacent striations in electron micrographs obtained earlier of four isolated rat myocytes (20). Because A-band position governs our method, sarcomere length was measured as the ultrastructural separation between the same side of the first M-line of adjacent A bands. Clumps of uniformly spaced striations were again found, and the differences between the length of the striations at the transitions was 0.045 ± 0.014 μm (±SD, $N = 42$ transitions). The latter compares well with the transition of 0.052 ± 0.014 μm that we find in living cells where the preparative shrinkage is not a factor. Transitions were not associated with a unique sarcomere length, and so activation does not provide a simple explanation. One possibility is that the transition represents asymmetry in each half sarcomere, such as slippage at the M-line. The curious organization of patches, however, still requires a long range influence that may be imposed by the cell's cytoskeletal or membrane networks. Mechanical evidence supporting this idea is discussed in the companion manuscript (18).

Contractile changes in the contrast between the striations

The chief virtue of the phase-locked loop method is that sarcomere length is measured rapidly and directly from individual striations. The sampling rate we used could be increased two- to threefold simply by doubling the numerical aperture (12), while the striations can be visualized by a form of microscopy (9) that eliminates many ambiguities in image formation. Specifically, image intensity with modulation contrast microscopy is related to the gradient of the refractive index (9). Thus, the striation's contrast represents the spatial derivative of the protein distribution in the myofibril. Accordingly, the degree of amplitude modulation of the video signal detects changes in the differences in the A- and the I band's refractive index (as related to the packing order of the myofilaments), the width of the A-I boundary (as related to the registration of the myofilaments), the width of the I band, or a combination of these effects at a given sarcomere length.

The magnitude and the time course of enhanced contrast during relengthening is similar to the changes in the intensity of the first order light diffracted from single cardiac cells (16, 23). However, contrast is not uniquely related to sarcomere length (Fig. 1 *E* and *F*), and so the contracting cardiac cell can not be treated as a simple grating. More specifically, the contrast behavior demonstrates that changes in the diffraction efficiency of the sarcomere must arise in its structural rearrangement rather than in the uniformity between diffracting elements. Cell volume changes are thought to be small, and both optical events are several orders of magnitude larger than any change which might be supposed to arise in changes in cellular birefringence. Moreover, when the sarcomere length is held constant in contraction the intensity of diffracted light does not change (cf. 22, Fig. 2). Thus, the simplest possibility is that the contrast

change reflects the disposition of myofibrillar protein due to the active sliding of the myofilaments (19). Plausible explanations might involve transient alterations in (*a*) the separation of filaments in the contractile lattice, (*b*) registration or skewing of the thick filaments, (*c*) the disposition of the myosin projections at the ends of the thick filament, or (*d*) an elastic or viscoelastic cytoskeletal restraint on intramyofibrillar protein distribution postulated in *a–c*.

Sarcomere dynamics

From observation of particles attached to frog atrial cells, it has been found that the initial phase of cardiac cell shortening may be unsteady or step-like (35). In contrast, single mammalian myocytes shorten smoothly as seen by light diffraction (16). However, diffractometry may not rule out the possibility that smooth sarcomere shortening behavior simply reflects a desynchronized or nonuniform motion between myofibrils (29). Our results show directly that smooth shortening is characterized by uniform and synchronous contractile activity. We caution that our finding does not bear directly on the basis for stepwise shortening (29) simply because it was not observed. In addition, one of the prerequisites for observation of stepwise behavior by diffractometry (an intriguing organization of the striation pattern) appears to be supported by our results.

Delays or pauses in relaxation and alternating contractile behavior

The pauses in relengthening were not seen in shortening (Fig. 7). Consequently, they can not be attributed to translation effects (1, 11) which, when tested, were found to be very small (Fig. 5). Restoring forces would be quite low at this point in contraction, but any potential effect of substrate adhesion is ruled out by the fact that these delays in relengthening are synchronous and, in some cases, characterized by additional shortening (Fig. 7*A*, contractions 10–11, *left*) that may represent a precursor to after-contractions. Intact cardiac cells expand laterally when they shorten, in which case patches of slightly different sarcomere lengths could be recruited into the sample population by moving vertically into or out of focus. However, a variation in sampling due to cell expansion or a change in its cross sectional shape does not explain synchrony during either shortening or relengthening.

The reproducible synchrony and good uniformity of the pause in relaxation, plus the fact that it first required a triggered contraction, preclude its origin in a truly spontaneous mechanism of release of intracellular calcium that may occur when contractile activity is less regular (3, 4, 14). This conclusion is reinforced by the fact that it is difficult to envision why synchrony would be maintained during transitions in the contractile behavior (Figs. 7 and 8). One possibility is that the ability of the sarcoplasmic reticulum to sequester calcium is impaired at slow stimulus rates, thus unmasking the presence of a late entry of calcium across the cell membrane (10). Other sources of calcium can be postulated, but any synchronization of sarcomere motions in relengthening requires either an element of membrane control of intracellular calcium dynamics or a myofibrillar effect in which its sensitivity to calcium increases as the sarcomere relengthens rapidly. Regardless of the mechanism, the existence of synchrony and uniformity of the pauses in relengthening in the isolated cell obviates the need to invoke desynchronization as a mechanism in the genesis of such pauses in relaxation.

In preliminary experiments, we have seen that spontaneous alterations in contractile shortening occur in voltage-clamped, internally dialyzed guinea pig myocytes after protocols of depolarization that favor elevation of the cells's calcium content (25). From measurements on the total length of isolated cells, it has been suggested that alternation in the amplitude of contraction can be also explained by asynchrony of intracellular calcium release mechanism (4). However, sarcomere shortening appears longitudinally synchronized and uniform over a wide range of adjustments in contraction (Fig. 8). Our measurements do not conflict with asynchronous calcium release when irregular contraction does indeed appear to be nonuniform (4). Our findings do not rule the possibility that activation may be radially nonuniform, but they do preclude subcellular desynchronization as a necessary explanation for some forms of irregular or unstable contraction.

APPENDIX

General circuit description

A block diagram of the circuit is shown in Fig. 2. The video signal from the photodiode array is directed through a variable-gain amplifier for automatic gain control (AGC) and a bandpass filter to attenuate out-of-band noise components of the video signal. The amplified and filtered video signal is then applied to the contrast ratio and sarcomere length measurement circuits.

1. Striation contrast. The contrast measurement circuit is composed of an amplitude detector, a gated lowpass filter, a sample-and-hold amplifier, and an output amplifier/buffer. The amplitude detector is simply a rectifier diode and a capacitor; it produces a voltage proportional to the instantaneous amplitude of the video signal. This amplitude signal is applied to a gated lowpass filter that operates as follows. At times other than the computation interval, the lowpass filter is gated OFF so that its output follows the amplitude signal without modification (no filtering is performed). During the computa-

tion interval, the lowpass filter is enabled, resulting in the attenuation of high-frequency components of the video signal which has the effect of smoothing (or averaging) the video signal. At the end of the computation interval the output of the gated lowpass filter is approximately proportional to the average video amplitude during the interval, and at this time the video amplitude is sampled by the following sample-and-hold amplifier. The sampled and held output provides the contrast ratio of the A and I bands, and is directed through an output amplifier/buffer that permits adjustment of its amplitude and DC offset. The sampled and held output is also used as the source of the automatic gain control (AGC) signal which controls the gain of the video input amplifier.

2. Sarcomere length. The sarcomere length measurement circuitry has been described previously (27) and so only its general operation will be discussed here. The amplified and filtered video is applied to an FM detector which produces a voltage directly proportional to the instantaneous frequency of the video signal. The FM detector is based upon a phase-locked loop circuit, which works by phase-locking the output of an internal voltage-controlled oscillator (VCO) to the video input, so that at all times the frequency of the internal VCO is exactly matched to the frequency of the video signal; the desired frequency output voltage can then be obtained directly from the VCO control voltage. The phase-locked loop used in our circuit was an LM 565C (National Semiconductor). The voltage controlled oscillator in our circuit was designed to have a center frequency of 17.00 kHz, which exists at a striation spacing of 1.86 μm. The 'hold-in' range (i.e., the frequency band for which the voltage-controlled oscillator tracks the sarcomere length signal) and the 'lock-range' (i.e., that frequency band in which the PLL can capture the input frequency) are ±60 and ±40%, respectively. The time to achieve lock with each scan of the video signal is 0.2 ms, or a value equivalent to the first ~7 μm of the image of the cardiac cell's striations (Fig. 1 *B*).

The output of the FM detector is applied to an integrator which, in conjunction with an analogue divider and another integrator, allows calculation of the average sarcomere length during the computation interval. Both integrators, initially reset to rest, are enabled at the onset of the computation interval. One integrates the frequency signal from the output of the FM detector, while the other integrates a constant voltage (producing an output corresponding to the integral of time over the computation interval). The analogue divider divides the integral of frequency into the integral of time, resulting in a voltage that is proportional to the average period of the video signal over the computation interval. This voltage, which is directly proportional to sarcomere length, is coupled to an amplifier whose gain is adjusted to produce an output of 1.00 V/μm. Two sample-and-hold amplifiers sample the sarcomere length at the end of each respective computation interval. The calibration grating indicated that the full relations between the phase error signal, ΦE (in V), the striation spacings in the test grating, $1.2 \leq ss \leq 3.0$ μm, and sarcomere length, *SL*, as measured from a digital voltmeter were: $\Phi E = 0.043\text{-}2.43/ss$, $ss = 0.09\text{-}2.225/\Phi E$, and $SL = 0.99ss$, where all coefficients of fit were $R^2 \geq 0.996$. At a striation spacing of 2.0 μm the scale factor, *k*, relating the fluctuation in the phase error to striation spacing is thus $d(ss)/d(\Phi E) = 2.225\,(1/\Phi E)^2 = 1.63$ μm/V.

The remaining circuitry produces the two window signals and the timing pulses needed for the sample-and-hold amplifiers. A window signal is produced by three monostable multivibrators connected in cascade. The photodiode array's SYNCH signal (which is a pulse that occurs at the beginning of each scan line) triggers the first monostable; the second monostable is triggered when the first times out. It is the second monostable that generates the actual window signal; its period is variable, permitting adjustment of the window width and thus the length of the sampled region. The first monostable functions as a variable delay that allows adjustment of the window's position relative to the cell. A third monostable, triggered at the end of the window, generates a 6 μs pulse that is used to drive the sample-and-hold amplifiers.

In our circuit there are two independent window generators, enabling two computation intervals per scan. Both computation intervals share the same calibration circuitry; the two window signals are logically ORed together for connection to the integrators. The two windows cannot overlap or else the integrators will not reset between measurements. (The contrast ratio is computed only once per scan and requires only one window signal.) A switch for scaling in the calibration signal permits use of microscope objectives of different magnification (×40 and 50).

3. Characteristic circuit response to change in striation spacing. Being dependent upon design parameters, the response of the circuit to a change of sarcomere length is determined solely by the characteristics of the phase-locked loop used in the FM detector. The phase locked-loop exhibits a response characteristic of a unity-feedback second order linear control system. The response time of such a system is directly related to its natural frequency ω_n and its damping factor, ζ, and it generally becomes faster for higher ω_n and lower ζ. Accordingly, our circuit was designed to exhibit a large value of 53273 rad/s for ω_n and a low value of 0.55 for ζ. A useful estimate of the step response of a second order system is the rise time, t_r, which is the time required for the output to change to within 10% of its final value following a step input. For a second order system with $\zeta = 0.55$, the rise time is approximately $t_r = 2/\omega_n = 2/(53272)$, or 37.5 μs. This interval spans 1.14 μm, which is three-fourths the shortest striation spacing expected in the isolated heart cell.

We especially thank Mr. Richard Tiberio of the NNF and his assistants Joe Limber and Jo McMillan for help in construction of the test grating. Nadine Stram, Dr. Hong Zhang, Gerard Siciliano, and Colin Devonshire provided technical assistance, and Mr. John Myers (Center for Bioengineering, University of Washington) kindly provided a schematic of his circuit (Myers et al., 1982) upon which our approach was based. We thank Dr. Douglas Christensen (University of Utah) for advice, Dr. Kenneth Roos (UCLA) for comments based upon an earlier version of this manuscript, Dr. Wayne Rasband (NIH) for software used in computer image analysis, and the referees for their challenge to evaluate the translation effects.

Supported, in part, by HL-21325. The work was performed in part at the National Nanofabrication Facility (NNF), which is supported by the National Science Foundation under Grant ECS-8619049, Cornell University, and industrial affiliates.

Received for publication 13 May 1991 and in final form 3 September 1991.

REFERENCES

1. Altringham, J. D., R. Bottinelli, and J. W. Lacktis. 1984. Is stepwise sarcomers shortening an artifact? *Nature (Lond.)*. 307:653–655.
2. Belardinelli, L., and G. Isenberg. 1983. Actions of adenosine and isoproterenol on isolated mammalian ventricular myocytes. *Circ. Res.* 53:287–297.
3. Berlin, J. R., M. B. Cannell, and W. J. Lederer. 1989. Cellular origins of the transient inward current in cardiac myocytes. *Circ. Res.* 65:115–126.
4. Capogrossi, M. C., and E. G. Lakatta. 1985. Frequency modulation

and synchronization of spontaneous oscillations in cardiac cells. *Am. J. Physiol.* 248:H412–H418.

5. Claes, A. V., N. M. DeClerck, E. R. Van Ocken, and D. L. Brutsaert. 1980. A new method for sarcomere length measurements. *Fed. Proc.* 39:1729.
6. DeClerck, N. M., V. A. Claes, E. R. Van Ocken, and D. L. Brutsaert. 1981. Sarcomere distribution patterns in single cardiac cells. *Biophys. J.* 35:237–242.
7. DeClerck, N. M., V. A. Claes, and D. L. Brutsaert. 1984. Uniform sarcomere behavior during twitch of intact single cardiac cells. *J. Mol. Cell Cardiol.* 16:735–745.
8. Determan, H., and F. Lepusch. The Microscope and its Application. Technical Manual. Ernst Leitz GMBH, Wetzlar, Germany. 512–696.
9. Hoffman, R. 1977. The modulation contrast microscope: principles and performance. *J. Microscopy.* 110:205–222.
10. Honore, E., C. E. Challice, P. Guibault, and P. Dupuis. 1986. Two components of contraction in guinea pig muscle. *Can. J. Physiol. Pharmacol.* 64:1153–1159.
11. Huxley, A. F. 1984. Sir Andrew Huxley comments. *Nature (Lond.).* 309:713–714.
12. Inoué, S. 1986. Videomicroscopy. Plenum Press, NY. p. 130.
13. Isenberg, G. 1982. Ca entry and contraction as studied in isolated bovine ventricular myocytes. *Z. Naturforsch.* 37:502–512.
14. Kort, A. A., M. C. Capogrossi, and E. G. Lakatta. 1985. Frequency, amplitude, and propagation velocity of spontaneous Ca^{++}-dependent contractile waves in intact adult rat cardiac muscles and isolated myocytes. *Circ. Res.* 57:844–855.
15. Krueger, J. W. 1988. Measurement and interpretation of contraction in isolated cardiac cells. *In* Biology of Isolated Adult Cardiac Myocytes. W. A. Clark, R. S. Decker, and T. K. Borg, editors. Elsevier Science Publishing Co., Inc.
16. Krueger, J. W., D. Forletti, and B. Wittenberg. 1980. Uniform sarcomere shortening behavior in isolated cardiac muscle cells. *J. Gen. Physiol.* 76:587–607.
17. Krueger, J. W., A. Denton, G. Siciliano, and R. C. Tiberio. 1989. Resolution and evaluation of asynchronous motions between sarcomeres in cardiac muscle cells. *Biophys. J.* 55:268*a*. (Abstr.)
18. Krueger, J. W., A Denton, and G. Siciliano. Nature of motions between sarcomeres in asynchronously contracting cardiac muscle cells. 61:145–160.
19. Krueger, J., and B. London. 1984. Contraction bands: differences between physiologically vs. maximally activated single heart muscle cells. *In* Contractile Mechanisms in Muscle. G. H. Pollack and H. Sugi, editors. Plenum Press. 119–134.
20. Krueger, J. W., and B. London. 1985. Morphological changes in the cardiac sarcomere during extreme passive and active shortening. *Biophys. J.* 47:130*a*. (Abstr.)
21. Krueger, J. W., B. London, and G. Siciliano. 1988. Separability of relaxation indices in isolated ventriculocytes. *In* Biology of Isolated Adult Cardiac Myocytes. W. A. Clark, R. S. Decker, and T. K. Borg, editors. Elsevier Science Publishing Co., Inc. 406–409.
22. Krueger, J. W., K. Tsujioka, T. Okada, C. Peskin, and M. Lacker. 1988. A 'give' in tension and sarcomere dynamics in cardiac muscle relaxation. H. Sugi and G. H. Pollack, editors. Molecular Mechanisms of Muscle Contraction. Plenum Press, New York.
23. Leung, A. F. 1983. Sarcomere dynamics in single myocardial cells as revealed by high-resolution light diffractometry. *J. Musc. Res. Cell. Mot.* 4:485–502.
24. London, B., and J. W. Krueger. 1986. Contraction in voltage-clamped, internally perfused single heart cells. *J. Gen. Physiol.* 84:475–505.
25. London, B., and J. W. Krueger. 1987. Some features of (i) contractile alternans & (ii) spontaneous, asynchronous contraction in the voltage-clamped, dialyzed heart cell. *Biophys. J.* 51:98*a*. (Abstr.)
26. Lundblad, A., H. Gonzalez-Serratos, G. Inesi, J. Swanson, and P. Paolini. 1986. Patterns of sarcomere activation, temperature dependence, and effect of ryanodine in chemically skinned cardiac fibers. *J. Gen. Physiol.* 87:885–905.
27. Myers, J., R. Tirosh, R. C. Jacobson, and G. H. Pollack. 1982. Phase locked-loop measurement of sarcomere length with high time resolution. *I.E.E.E. Trans. BioMed. Eng.* 29:463–466.
28. Pollack, G. H. 1984. Is stepwise sarcomere shortening an artifact?—a response. *Nature (Lond.).* 309:712–713.
29. Pollack, G. H. 1986. Quantal mechanisms in cardiac contraction. *Circ. Res.* 59:1–8.
30. Reiser, G., R. Sabbadini, P. Paolini, M. Fry, and G. Inesi. 1979. Sarcomere motion in isolated cardiac cells. *Am. J. Physiol.* 236:C70–C77.
31. Roos, K. P., and A. J. Brady. 1982. Individual sarcomere length determination from isolated cardiac cells using high-resolution optical microscopy and digital image processing. *Biophys. J.* 40:233–244.
32. Roos, K. P. 1987. Sarcomere length uniformity determined from three-dimensional reconstruction of resting isolated heart cells striations patterns. *Biophys. J.* 52:317–327.
33. Roos, K. P., and A. J. Brady. 1991. Osmotic compression and stiffness changes in relaxed skinned cardiac myocytes in PVP-40 and Dextran T-500. *Biophys. J.* 58:1273–1283.
34. Schnapp, B. J., J. Gelles, and M. Sheetz. 1988. Nanometer-scale measurements using video light microscopy. *Cell Motility and the Cytoskeleton.* 10:47–53.
35. Tameyasu, T., T. Toyoki, and H. Sugi. 1985. Nonsteady motion in unloaded contractions of single frog cardiac cells. *Biophys. J.* 48:461–465.